

Doping Metal Ions into $\text{Cs}_2\text{AgInCl}_6$ Halide Double Perovskites

A thesis submitted to

Indian Institute of Science Education and Research, Pune

for partial fulfillment of

BS-MS Dual Degree Program



By

Nila Nandha K (20131027)

Under the supervision of

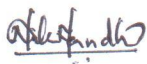
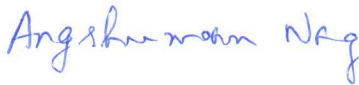
Dr. Angshuman Nag

Assistant Professor, Department of Chemistry

Indian Institute of Science Education and Research, Pune

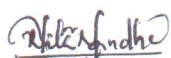
Certificate

This is to certify that this dissertation entitled 'Doping metal ions into $\text{Cs}_2\text{AgInCl}_6$ halide double perovskite' towards the partial fulfillment of the BS-MS dual degree programme at the Indian Institute of Science Education and Research Pune represent the work carried out by Nila Nandha K at IISER Pune under the supervision of Dr. Angshuman Nag, Assistant Professor, Department of Chemistry during the academic year 2017-2018.

Date : 14/03/2018	 Nila Nandha K	 Dr. Angshuman Nag
Place : Pune	5 th year student	Assistant Professor
	BS-MS dual degree	Department of Chemistry
	IISER Pune	IISER Pune

Declaration

I hereby declare that the matter embodied in the report entitled 'Doping metal ions into $\text{Cs}_2\text{AgInCl}_6$ halide double perovskite' are the results of the work carried out by me at the Department of Chemistry, IISER Pune under the supervision of Dr. Angshuman Nag and the same has not been submitted elsewhere for any other degree.



Date : 14/03/2018

Nila Nandha K

Place : Pune

5th year Student

BS-MS dual degree

IISER Pune



Dr. Angshuman Nag

Assistant Professor

Department of Chemistry

IISER Pune

Acknowledgments

This thesis would not have been possible without a few individuals who in one way or another extended their guidance and support to carry out and complete this work.

First and foremost, I'd like to extend my sincere gratitude towards my supervisor, **Dr. Angshuman Nag**, IISER Pune for providing me an opportunity to carry out my fifth year MS thesis project under his guidance. His remarkable vision, deep knowledge, optimistic nature and encouraging supervision have been my inspiration to move forward with my work. I'd also like to thank my TAC member, **Dr. Pramod Pillai** (Assistant professor, IISER Pune) for his unfailing support through out my project.

I'd like to thank Vikas for helping me initially with solid state PL measurements. I'd also like to thank Gayathri for UV measurements, Dr. Jayakannan's Lab for providing TGA facility and SAIF (IIT Bombay) for ICP-AES and EPR measurements. I'd like to acknowledge Abhishek, Jaya, Tariq and Nancy for valuable discussions, assistance and constant support and motivation throughout the course of my project. I'd like to thank all other lab members for their encouragement and truly it was a pleasure working alongside them. Last but not the least, I'd like to thank my family and my friends Nasreen, Jesil, Keerthana and Aathira for providing me unceasing support throughout my BS-MS course.

Table of Content

Abstract

Chapter 1: Doping metal ions into $\text{Cs}_2\text{AgInCl}_6$ halide double perovskites.....9

Part I: Synthesis and luminescence of Mn-doped $\text{Cs}_2\text{AgInCl}_6$ halide double perovskite

1. Introduction.....	10
2. Methodology.....	13
2.1 Materials.....	13
2.2 Synthesis of Mn^{2+} doped $\text{Cs}_2\text{AgInCl}_6$	13
2.3 Instrumental characterization.....	14
2.3.1 Inductively Coupled Plasma Atomic Emission Spectroscopy.....	14
2.3.2 X-ray Diffraction (XRD).....	14
2.3.3 Field Emission Scanning Electron Microscope (FESEM).....	15
2.3.4 UV-Visible Diffuse Reflectance Spectroscopy.....	15
2.3.5 Steady state PL and PL decay Dynamics.....	16
2.3.6 Electron Paramagnetic Resonance (EPR) Spectroscopy.....	16
2.3.7 Thermogravimetric Analysis (TGA).....	17
3. Results and Discussion.....	17
3.1 Crystal structure and molecular orbital diagram.....	17
3.2 Structural analysis and morphology.....	18
3.3 Optical characterization.....	20
3.4 EPR studies.....	24
3.5 Stability studies.....	25
4. Conclusion.....	26

Part II: Attempts to dope lanthanide metal ions (Eu^{2+} and Sm^{3+}) into $\text{Cs}_2\text{AgInCl}_6$ halide double perovskite crystal

1. Introduction.....	27
2. Methodology.....	29
2.1 Materials.....	29

2.2 Synthesis.....	29
2.3 Instrumental characterization.....	29
3. Results and Discussion.....	30
3.1 Structural characterization.....	30
3.2 Optical characterization.....	31
4. Conclusion.....	32
Part III: Attempt to synthesize Cs ₂ AgIn(Cl/Br) ₆ mix halide double perovskite	
1. Introduction.....	33
2. Methodology.....	34
2.1 Materials.....	34
2.2 Synthesis.....	35
2.3 Instrumental characterization.....	35
3. Results and Discussion.....	35
3.1 Structural characterization.....	35
3.2 Optical characterization.....	36
4. Conclusion.....	37
References.....	38

List of Figures

1. Schematic of cation transmutation strategy.....	11
2. Schematic representation of Mn-doped Cs ₂ AgInCl ₆ synthesis protocol.....	14
3. Structure and energy band diagram of Cs ₂ AgInCl ₆	17
4. Morphological and structural analysis of Mn-doped Cs ₂ AgInCl ₆	19
5. Optical characterization and Emission mechanism of Mn-doped Cs ₂ AgInCl ₆	21
6. PL decay dynamics of Mn-doped Cs ₂ AgInCl ₆	23
7. EPR spectra of Mn-doped Cs ₂ AgInCl ₆	25
8. Stability studies; XRD and TGA data.....	26
9. Structural analysis of Lanthanide-doped Cs ₂ AgInCl ₆	30
10. Optical characterization of Lanthanide-doped Cs ₂ AgInCl ₆	31
11. Octahedral factor calculated for Cs ₂ AgInX ₆ (X- Cl, Cl/Br, Br, Br/I, I).....	34
12. Structural characterization of Cs ₂ AgIn(Cl/Br) ₆ mix HDP.....	36
13. Optical characterization of Cs ₂ AgIn(Cl/Br) ₆ mix HDP.....	37

List of Tables

1. PL decay fitting parameters for Mn-doped Cs ₂ AgInCl ₆	24
---	----

Abstract

Lead halide perovskites have been rising as a potential candidate for photovoltaic (PV) and light emitting diode applications due to their impressive optical and optoelectronic properties. However, their commercialization confronts major issues like moisture and thermal instability and Pb toxicity. Recent development of lead-free halide double perovskites (HDPs), $A_2B^I C^III X_6$ by substituting the divalent cation Pb^{2+} with a monovalent and a trivalent cation have been suggested to overcome the above concerns. But most HDPs have either indirect or wide band gaps with weak photoluminescence (PL) emissions limiting their optical applications. Recently reported $Cs_2AgInCl_6$ HDPs exhibit direct band gap as well as inherent crystal stability but they have a wide band gap (3.5 eV). They also have a very less intense, broad, defect mediated emission in the lower energy region of visible spectrum. Hence tailoring the optical emission of $Cs_2AgInCl_6$ was necessary. Here I report the synthesis and characterization of metal ion doped $Cs_2AgInCl_6$ double perovskites. Doping of Mn^{2+} transition metal ions into the $Cs_2AgInCl_6$ host lattice imparted an intense emission at red region (632 nm) due to the spin forbidden ${}^4T_1 - {}^6A_1$ transition of Mn d electrons. PL decay for doped samples revealed sub millisecond lifetime accounted for the spin forbidden transitions of isolated Mn^{2+} dopants. A hyperfine splitting constant of 8.5 mT confirms the incorporation of Mn^{2+} into $Cs_2AgInCl_6$ lattice. Lanthanide ions doping (Eu^{2+} and Sm^{3+}) were carried out expecting sharp and intense multicolor emission in $Cs_2AgInCl_6$ host. Also $Cs_2AgIn(Cl/Br)_6$ mix HDP synthesis was attempted for developing a direct band gap material with suitable band gap for PV application.

Part I

Synthesis and luminescence of Mn-doped Cs₂AgInCl₆ halide double perovskites

1. Introduction

Lead halide perovskites (LHP's) with a general formula ABX₃ (A– CH₃NH₃⁺ (Methylammonium, MA), CH(NH₂)₂⁺ (Formamidinium, FA), Cs⁺; B- Pb, X– Cl⁻, Br⁻, I⁻) have become the centre of active research in the field of photovoltaic (PV) and optoelectronics for the past few years¹. Their unique intrinsic properties like high absorption coefficient, bright and narrow band edge emission, high carrier mobility, long diffusion length, colour tunability and solution processability have enabled LHP's to be used in various devices which displays high operational efficiency and economically feasible fabrications². But their large scale commercialization is compromised by two major reasons; lack of thermal and air stability and lead toxicity³.

Design and fabrication of different optoelectronic devices requires semiconducting materials which are stable for years under the relevant radiation conditions for the commercial viability of the product. For example, in devices like Light Emitting Diode (LED's), the emitter materials have to be in close contact with powerful ultraviolet (UV) flux which transfers heat energy to them during the functional time period (minutes to hours)⁴. PV devices like solar cells, in addition needs air and moisture stability for a long operational lifespan. However, LHP's lack air as well as thermal stability to be utilized in the above devices³. Though the exact reason is unclear, lack of intrinsic thermodynamic stability due to very small lattice formation energy could be the cause of LHP's easy degradation⁴. Methylammonium (MA) based perovskites have shown volatile nature even at 85 °C and degrades readily on moisture exposure despite their 22.1% power conversion efficiency (PCE) reported so far⁵. Replacing small organic cations like MA or FA with inorganic Cs⁺ have significantly improved the stability issues but could not obliterate these issues completely⁶.

According to the Restriction of Hazardous Substances (RoHS) directive put forward by the European Union, the total amount (by weight) of heavy toxic metals like Cd or Pb should be less than 100 and 1000 parts per million (ppm) respectively in all electronic devices. This has been taken forward by countries like USA and is a major constrain for commercializing lead halide perovskites. The problem of lead toxicity becomes severe in solar cell applications since LHPs decompose readily in rain water forming the water soluble carcinogen PbI_2 and can pollute water bodies raising environmental concerns⁶. Complex encapsulation of LHPs in devices may address the problem but increases the production cost enormously. Replacing B site cation is not an easy solution since they are directly involved in determining the crystal structure and energy diagrams of halide perovskite materials⁷. Homovalent substitution of Pb^{2+} with Sn^{2+} or Ge^{2+} lead to the oxidation of the same into their respective +4 stable states and make them unsuitable for device applications⁸. Replacing Pb^{2+} with Sb^{3+} or Bi^{3+} resulted in zero dimensional (0D) or one dimensional (1D) perovskites structures due to the vacancy formation in the crystals owing to the difference in the oxidation states of Pb from bismuth or antimony. The low dimensional perovskites thus formed exhibit high exciton binding energy, low photoluminescence (PL) quantum yield, heavy charge carrier masses etc⁹ and is not suitable for optoelectronic device applications. Therefore, it is of great importance to find an alternate material for lead halide perovskite with less toxic elements and high crystal

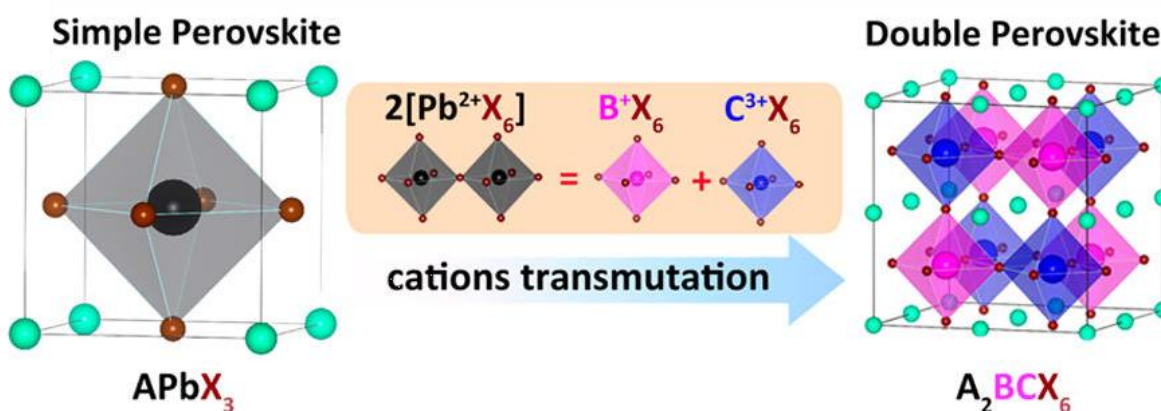


Figure 1: Schematics showing the cation transmutation of 2 Pb^{2+} ions by a monovalent (B^+) and trivalent (C^{3+}) cations. (figure adapted with permission from Zhao et al.¹⁰ Copyright 2017, American Chemical Society)

stability along with the excellent properties of LHPs.

Recently, Lead free halide double perovskites (HDP's) with a general formula $A_2B^I C^{III} X_6$ (A- Cs^+ ; B^I- monovalent cation Au^+ , Ag^+ , Tl^+ , Cu^+ ; C^{III}- trivalent cation Bi^{3+} , Sb^{3+} ; X- Cl^- , Br^- , I^-) have been proposed as an alternate for $CH_3NH_3PbI_3$ ¹¹. Oxide double perovskites are a well studied system with high air and thermal stability. Heterovalent substitution of 2 Pb^{2+} ions in a simple perovskite crystal with a monovalent and a trivalent cation maintaining the charge neutrality forms a 3D double perovskite structure as shown in figure 1. It has been reported that most of the properties exhibited by LHP's including the defect tolerant nature arise from the $6s^2 6p^0$ electronic configuration of lead. In order to maintain the ns^2 configuration, the possible transmutation elements for HDP's would be isoelectronic Bi^{3+} and Sb^{3+} ¹¹. Recently reported $Cs_2AgBiCl_6$ and $Cs_2AgBiBr_6$ exhibited high thermal and air stability as well as suitable band gaps (2.77 eV and 2.19 eV respectively)¹² for tandem PV applications. However they have an indirect bandgap due to a horizontal shift of valence band maxima from Γ point in the energy band diagram. This push must have happened because of the interaction of Bi s states with directional Ag d states¹³. Further computational studies removing Bi s states from energy diagram showed a direct band gap suggesting the role of Bi^{3+} in the indirect nature of Cs_2AgBiX_6 band gap¹³. Indirect band gap results in low optical absorption coefficients for the material and is less preferred for PV devices. Replacing Bi^{3+} completely with In^{3+} , the so developed $Cs_2AgInCl_6$ exhibited direct band gap as well as inherent stability but they have a wide band gap (3.3 eV)¹³ which is not suitable for highly efficient light absorption for devices like solar cells. $Cs_2AgInCl_6$ halide double perovskite with suitable band gap engineering and subsequent tailoring of optical properties is expected to show promise in future device applications.

In part I, I report the synthesis and characterization of $Cs_2AgInCl_6$ double perovskites with Mn^{2+} doping in order to improve PL emission from the material. Doping of materials is an efficient and well explored method to tailor different properties of the host such as optical properties, magnetic properties etc. Incorporating Mn^{2+} into the inorganic crystal lattice of different metal halide perovskites have been proven as an effective method to introduce a broad and intense PL emission in the orange-red region of visible spectrum

as a result of an atomic transition from ${}^4T_1 - {}^6A_1$ energy states of Mn^{2+} ions¹⁴. $Cs_2AgInCl_6$ exhibits a very less intense, broad, defect mediated emission in the red region of visible spectrum. Doping of Mn^{2+} into the $Cs_2AgInCl_6$ host lattice enhanced the emission at the red region through the mediation of Mn^{2+} states by an efficient energy transfer mechanism from the host. Since both host and dopant have an emission in the red region, there is only a single highly intense red emission in the Mn^{2+} doped $Cs_2AgInCl_6$ double perovskites. This enhanced red emission along with detailed future studies makes the material a promising candidate for application in Light Emitting Diodes (LED's).

2. Methodology

2.1 Materials

Hydrochloric acid (HCl, Purity-37 wt %), Cesium chloride (CsCl, 99.9%), Indium trichloride ($InCl_3$, Anhydrous powder, 99.999%), Silver chloride (AgCl, 99.999%) and Manganese chloride ($MnCl_2$, 99%) were purchased from Sigma Aldrich Chemicals. Ethanol (>99.9%) and Acetone (>99.9%) were purchased from Rankem Chemicals. All the precursors were used as received without further purifications.

2.2 Synthesis of Mn^{2+} doped $Cs_2AgInCl_6$

Undoped and Mn^{2+} doped $Cs_2AgInCl_6$ was synthesized by an acid precipitation synthesis protocol that has been reported recently with slight modifications¹³. Figure 2 shows a schematic representation of the experimental procedure. For undoped sample, 0.5 mmol of AgCl and $InCl_3$ each were taken in 3 ml 10M HCl. The vial containing the above precursors was kept heating at 72 °C under vigorous stirring. Later on 1 mmol of CsCl was added under stirring, forming a pale white precipitate immediately. The mixture was kept heating for another 20 min to ensure complete reaction of all the precursors. Afterwards the precipitate was filtered, washed with ethanol and dried in oven at 100 °C overnight. For Mn^{2+} doped samples, $MnCl_2$ was used as the manganese precursor. For doping 0.1% of Mn^{2+} , 0.01 mmol (0.05 mmol for 0.3% doping, 0.1 mmol

for 0.9% doping) of MnCl_2 was taken along with rest of the precursors. The synthesizing protocol was similar as described above.

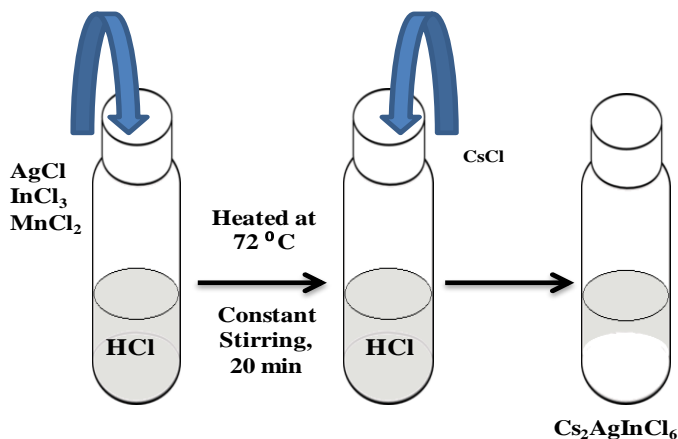


Figure 2: Schematic representation of the synthesis of $\text{Cs}_2\text{AgInCl}_6$ halide double perovskite using acid precipitation method.

2.3 Instrumental Characterization

2.3.1 Inductively Coupled Plasma Atomic Emission Spectroscopy (ICP-AES)

ICP-AES analysis is an emission spectroscopic technique used to detect elemental composition of a given sample. High temperature argon plasma is used to excite electrons from the ground state to excited states and when they return back, emits electromagnetic radiations of specific wavelength. This wavelength depends upon electronic configuration of different elements and thus is element specific. Intensities of different wavelength for different elements are collected simultaneously (depends upon ICP-AES instrument). These data are then compared with the calibration plot of reference samples with previously known elemental concentrations.

ICP- AES analysis was carried out using ARCOS simultaneous ICP spectrometer, SPECTRO Analytical Instruments GmbH, Germany. All samples were prepared in acid water mix at a concentration not more than 10 parts per million (ppm) for each sample. Dopant element concentration was kept at 100 ppm for better analysis. All calculations on the latter samples were done normalizing by a factor of 10.

2.3.2 X-ray Diffraction (XRD)

XRD gives information about the crystal structure, composition of crystals, size of the particles, lattice parameter etc. The main principle of XRD pattern formation is based on Bragg's condition,

$$2d \sin\theta = n\lambda$$

where d is the interplanar distance of lattice planes in crystal, θ is the angle of diffraction and λ is the wavelength of incident X-ray. Satisfying above condition leads to a constructive interference of x ray's diffracted from crystals. Scanning through a range of 2θ values, all possible directions of X-ray diffraction from a particular crystal structure is identified and recorded as XRD pattern.

Powder XRD measurements were carried out in a 2θ range of 10° to 80° using a Bruker D8 Advanced X-ray Diffractometer equipped with Cu $K\alpha$ radiation of wavelength 1.54 \AA . All solid samples were grounded into fine powder before analysis. The measurements were done on a glass substrate at a scan speed of 0.1.

2.3.3 Field Emission Scanning Electron Microscopy (FESEM)

FESEM technique gives important information about the surface morphology and elemental composition of crystals. They differ from conventional SEM as they are equipped with a narrow beam in electron gun. They can be operated at high electron energies and thus provides a better resolution of images. FESEM measurements were carried out using Zeiss Ultra Plus Field Emission SEM instrument. All samples were loaded evenly on $2 \text{ mm} \times 1 \text{ mm}$ carbon tape and degassed for 10 minutes before analysis.

2.3.4 UV-Visible diffuse reflectance spectroscopy

Diffuse reflectance spectroscopy is the study of incident light scattered in all direction from a samples. When light is incident upon solid samples like single crystals or polycrystalline, a small amount of light gets reflected in all direction due to surfaces, grain boundaries and multiple refractions (specular refection). Another part gets transmitted through the crystals and is not absorbed by the sample on travelling course. On reaching the surface they gets scattered in all direction forming diffuse reflectance.

The diffuse reflectance spectra is used to determine the band gap of material using a function called Kubelka- Munk function³¹ defined as,

$$F(R) = \frac{(1-R)^2}{2R} = K/S$$

R, K and S are reflection, absorption and scattering coefficients respectively. UV-Visible diffuse reflectance spectroscopy is carried out by Shimadzu UV 3000 600Plus UV-Vis/NIR Spectrophotometer in the range of 200 nm- 800 nm. All samples were ground into fine powder before measurements.

2.3.5 Steady state PL Spectroscopy and PL decay dynamics.

Photoluminescence (PL) is the process of emission of light by a sample on relaxation from singlet excited state to ground state via radiative mechanism. The energy of light emitted is lower compared to the absorbed energy. This typically occurs in nanosecond (ns) timescale depending upon the materials and lattice temperature. PL emission is measured in the steady state mode where the sample is excited and the decay of PL is counted as per the energy of photons. PL lifetime decay measurements were carried out using time resolved mode where the decay in PL is measured with respect to time.

All PL measurements were carried out using FLS980 fluorescence spectrometer, Edinburg Instruments. Lifetime decay measurements were done using a microsecond flash lamp of 100 W power. All decay plots were fitted with inbuilt exponential fitting package in OriginPro 8.5 data analyzing software.

2.3.6 Electron Paramagnetic Resonance (EPR) Spectroscopy

EPR spectroscopy is a powerful technique to determine detailed information about different atomic or molecular systems, especially the unpaired electrons present in them. When an external magnetic field is applied to an atom or molecule, the electronic energy levels of unpaired electrons would split into different energy levels. The atom can be excited into this split levels by absorbing microwave frequency depending upon the splitting energy. An EPR spectrum is recorded as per the number of such magnetic resonance absorptions. The spectra are sensitive to the local environment of unpaired

electron. EPR measurements were carried out using a JES- FA200 ESR spectrometer (JEOL, Japan) in X band frequency range.

2.3.7 Thermo-Gravimetric Analysis (TGA)

TGA is a thermal analysis method in which the sample weight loss is recorded with change in temperature over time. This is a powerful method to analyze phase change, decomposition temperature etc. of samples. All TGA measurements were carried out using a Perkin Elmer STA 6000. Samples were heated in a temperature range of 30-800 °C at a 10 °C/ min heating rate under inert atmosphere.

3. Results and Discussion

3.1 Crystal structure and Molecular orbital diagram

Figure 3a shows a schematic of the crystal structure of $\text{Cs}_2\text{AgInCl}_6$. It crystallizes in a face centered cubic structure with an $Fm\bar{3}m$ space group and a lattice parameter $a=10.20 \text{ \AA}$ as reported earlier¹³. The oxide counterparts of HDP's are also known to show

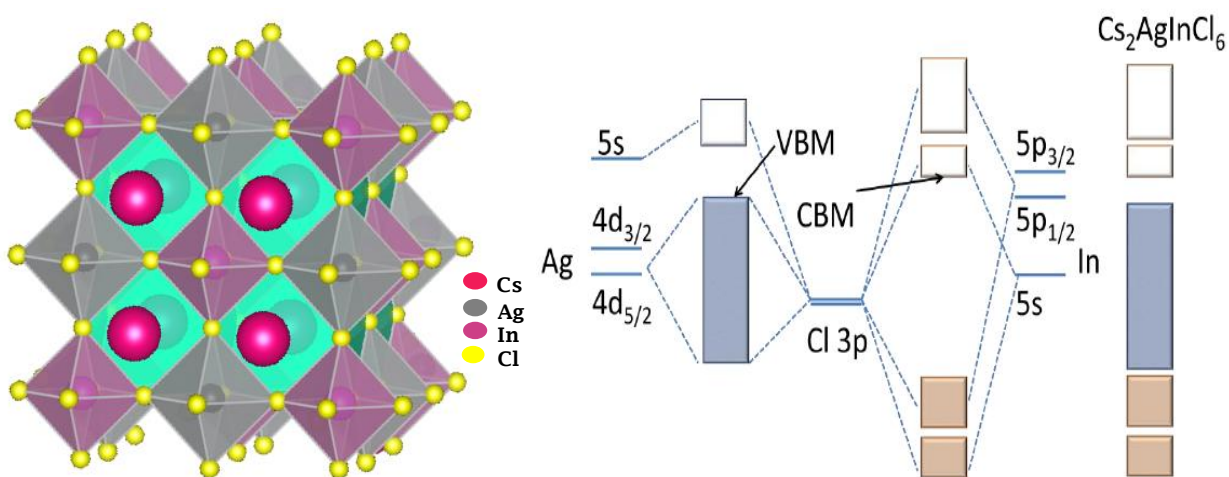


Figure 3 a) Schematic of $\text{Cs}_2\text{AgInCl}_6$ double perovskite structure in polyhedral representation. InCl_6 and AgCl_6 octahedra are represented by magenta and grey colour respectively. In^{3+} and Ag^+ (magenta and grey spheres) occupy the center of their octahedra and Cs^+ (pink spheres) occupy the cubeoctahedral voids. b) Schematic of molecular orbital diagram of $\text{Cs}_2\text{AgInCl}_6$ showing bonding and anti bonding bands (figure adapted with permission from Tran et.al¹⁵. Copyright 2017, Royal Society of Chemistry).

a similar type of rock-salt orderings. It consists of $[\text{AgCl}_6]$ and $[\text{InCl}_6]$ octahedra alternating in all the directions forming a 3 dimensional (3D) network with Cs^+ ions occupied at the center of the cubeoctahedral space. $\text{Ag}^+ / \text{In}^{3+}$ occupies at the center of their respective octahedra and form ionic bonds with the corner sharing Cl^- ions, directly influencing the energy band diagram and electronic structure. On the other hand, Cs^+ ions are held together in the voids by Vander Val's attraction and are not bonded chemically with the surrounding octahedra. The small size of A site cation directly influences the 3D crystal structure formation in double perovskites like in the case of LHP's. The ionic radii of Ag^+ (1.15 \AA) and In^{3+} (0.8 \AA) in the octahedral environment is in agreement with Pb^{2+} (1.19 \AA) in LHP's.

Figure 3b shows schematics of the molecular orbital diagram of $\text{Cs}_2\text{AgInCl}_6$ reported by Tran et al¹⁵. From this diagram it is clear that the valence band maximum (VBM) given as blue shaded box is predominantly made up of anti bonding Ag d states and Cl p states. At the same time, conduction band minimum (CBM) shown in non shaded box is made up of anti bonding In s states and Cl p states. Bi^{3+} based double perovskites namely $\text{Cs}_2\text{AgBiCl}_6$ or $\text{Cs}_2\text{AgBiBr}_6$ has a CBM mainly constituting anti bonding Cl p states and Bi p states and VBM with anti bonding Ag d states and Cl p states. But the Bi s state in the VBM interacts with directional Ag d states and pushes the VBM away from Γ point in the energy band diagram of Bi/ Ag based double perovskites resulting in an indirect band gap¹³. Unlike them $\text{Cs}_2\text{AgInCl}_6$ have a direct band gap. Thus replacing bismuth completely with indium causes a shift from indirect to direct band gap.

3.2 Structural analysis and Morphology

ICP-AES analysis confirmed 0.1, 0.3 and 0.9% of Mn^{2+} in the prepared samples for an added precursor of 1, 5 and 10% with respect to the Ag and In content by weight. Figure 4a shows the FESEM images of 0%, 0.1%, 0.3% and 0.9% Mn^{2+} doped $\text{Cs}_2\text{AgInCl}_6$. Both doped and undoped samples have a similar morphology as seen in the figure. Crystals are multi faceted with an average size ranging below $10 \mu\text{m}$. Zhou et al.¹⁶ have reported an average crystal size ranging between 5 to $12 \mu\text{m}$ with a rhombic dodecahedral shape recently which agrees with our observations.

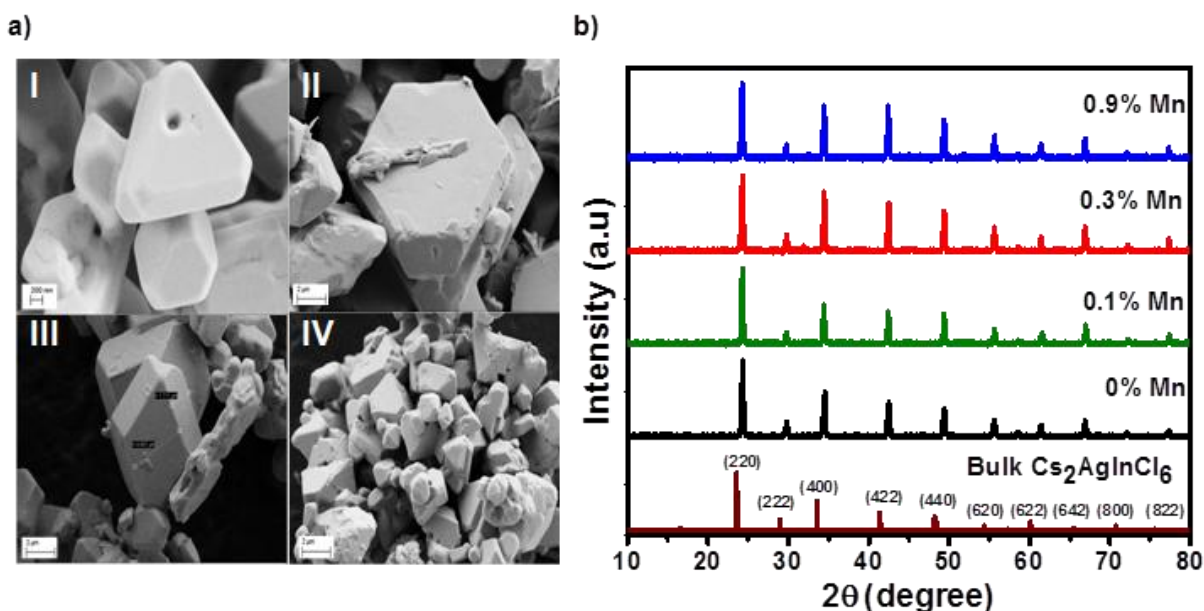


Figure 4 a) Typical FESEM images of I) 0% II) 0.1% III) 0.3% IV) 0.9% Mn-doped $\text{Cs}_2\text{AgInCl}_6$. All the magnification range is 2 μm , except for 0% (200 nm). b) Powder XRD patterns of undoped (0%) and Mn-doped (0.1%, 0.3%, 0.9%) samples. All spectra are vertically shifted for a better view.

XRD patterns of undoped (0%) and doped (0.1%, 0.3%, 0.9%) given in Figure 4b clearly agrees with the already reported DFT model of $\text{Cs}_2\text{AgInCl}_6$ ¹³. No additional peaks are observed in the XRD patterns of any samples suggesting the absence of Mn related impurities. Also no peaks of AgCl are observed suggesting the absence of AgCl residues in the samples. Hence, the synthesized crystals are pure and free from impurities like un reacted precursors or secondary side products. Thus pure and homogenously sized $\text{Cs}_2\text{AgInCl}_6$ crystals can be synthesized using the adapted acid precipitation method. The Shannon radii of Mn^{2+} in an octahedral environment is 0.83 Å which is relatable to Ag^+ (1.15 Å) and In^{3+} (0.8 Å) in the same conditions. Henceforth, doping Mn^{2+} into $\text{Cs}_2\text{AgInCl}_6$ crystal is expected to replace either Ag^+ or In^{3+} from their respective octahedra or both and thereby a slight reduction in octahedral size. Such a change in the lattice parameter will be reflected in XRD pattern in the form of 2θ shifting to higher angles. Interestingly there is no significant shift in the XRD peaks of doped samples from the undoped ones suggesting that a very little amount of Mn^{2+} is incorporated into the crystal lattice which agrees with our ICP-AES results. This small doping percent (<1%) may be due to a poor Mn^{2+} doping tendency in $\text{Cs}_2\text{AgInCl}_6$ crystal

structure. Thus undoped and doped $\text{Cs}_2\text{AgInCl}_6$ samples show similar structural and morphological characteristics.

3.3 Optical Characterization

The Uv-vis diffuse reflectance spectra were measured and converted into absorption spectra (figure 5a) using Kubelka-Munk function³⁰ for all the synthesized powder samples; 0%, 0.1%, 0.3% and 0.9% Mn^{2+} doped $\text{Cs}_2\text{AgInCl}_6$. From the absorption spectra, it is seen that $\text{Cs}_2\text{AgInCl}_6$ is a wide band gap material with an absorption in the near UV region. The absorption onset is seen from 350nm (3.5 eV) for the undoped and doped samples. Thus the optical band gap of $\text{Cs}_2\text{AgInCl}_6$ is estimated at 3.5 eV for both undoped and doped samples in spite of Mn^{2+} ion doping. The small amount of Mn incorporated (<1%) does not show significant change in band gaps. All samples show a sharp absorption onset at 350 nm which is a characteristic of direct band gap material. Inset of Figure 5a shows the photograph of undoped and doped (0.9% Mn) samples under ambient light. The samples appear white which confirm the fact that they do not absorb any light in the visible region.

Figure 5b displays steady state PL emission spectra of undoped (0%) and doped (0.1%, 0.3% and 0.9%) samples. The undoped host sample shows a PL peak at 619 nm with a large FWHM of 186 nm (0.6 eV) when excited at 330 nm above the band edge. A high stokes shift of 329 nm (2.3 eV) suggest that it is not a band edge emission but can be mediated by the defect states present within the energy gap. On contrary, Mn^{2+} doped samples have an intense PL emission centered at 632 nm which is slightly (~13 nm) red shifted from the undoped samples. Also the peaks are well defined and have an FWHM of ~100 nm (0.3 eV) which is lower than the broader PL peak observed for undoped samples. This FWHM value of ~100 nm corresponds to previously reported Mn emissions^{14 17}.

Undoped $\text{Cs}_2\text{AgInCl}_6$ has a very less PL intensity and a broadened PL emission which can be attributed to deep trap states within the energy gap of host $\text{Cs}_2\text{AgInCl}_6$ and are the main centers of non radiative recombinant processes. As a result a defect mediated emission at lower energies is observed instead of a band edge emission. This is proved

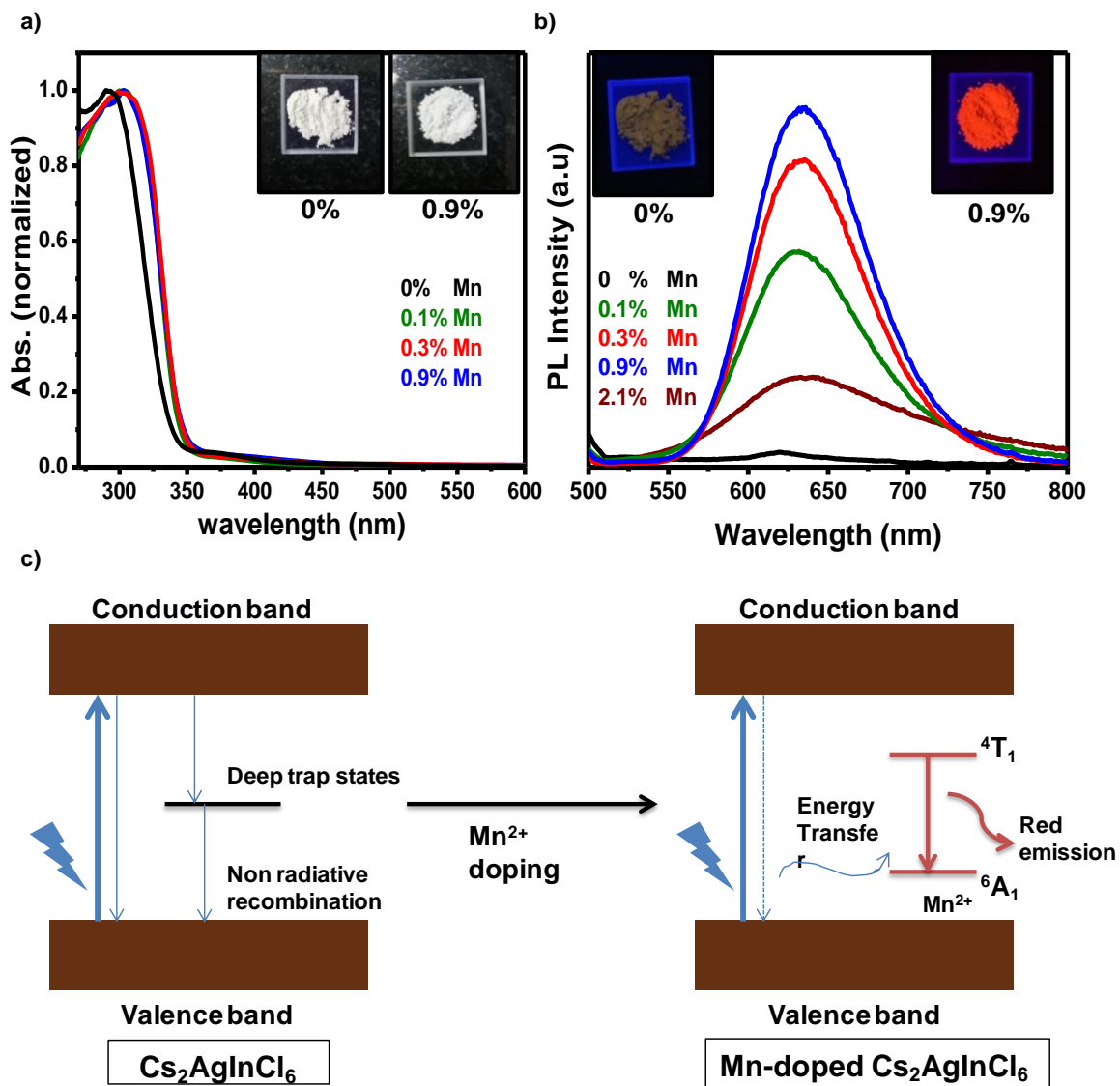


Figure 5a) UV-Visible absorption spectra of undoped (0%) and Mn-doped (0.1, 0.3 and 0.9%) $\text{Cs}_2\text{AgInCl}_6$ samples. The spectra are normalized at the absorption maximum for all samples. b) Steady state PL emission spectra of undoped and doped samples at 330 nm excitation wavelength. Photographs of 0% and 0.9% Mn-doped samples under ambient light and UV illumination (254 nm) are shown in the inset of figure a) and b) respectively. c) Schematic showing the proposed emission process in undoped (left) and Mn-doped (right) $\text{Cs}_2\text{AgInCl}_6$ halide double perovskites.

by a large Stokes shift of 329 nm observed for undoped sample. Figure 5c presents a schematic of emission mechanism in undoped and Mn-doped $\text{Cs}_2\text{AgInCl}_6$. In doped

materials, excited state energy from host gets transferred to Mn^{2+} d states and excites the ${}^6\text{A}_1$ ground state of Mn^{2+} . The intense luminescence in Mn-doped samples can be assigned to this forbidden ${}^4\text{T}_1 - {}^6\text{A}_1$ d-d transition of Mn^{2+} sensitized by the host $\text{Cs}_2\text{AgInCl}_6$. Doping decreases the emission via trap states and increases the dopant emission by an efficient energy transfer mechanism from host to dopant energy levels. The ${}^4\text{T}_1 - {}^6\text{A}_1$ inner core atomic like transition interacts less with non radiative defects in the host lattice. This can also be the reason behind the enhanced PL intensity observed for Mn-doped emissions in comparison with prior reports^{18 19 20}. When the samples are excited with energies lower than the band gap, no emission was observed. This suggests the usual emission mechanism of Mn d electron via the energy transfer from the excited metal halide perovskite host. This d-d transition results in a ~10 fold intense PL peak in the red region for doped samples compared to the undoped sample in figure 5b.

Figure 5b also presents a comparison of Mn d-d emission intensity with different Mn^{2+} concentration. When the concentration of Mn^{2+} is increased from 0.1% to 0.9%, the emission band becomes stronger and intense. But as the concentration is increased above 0.9%, the PL intensity decreases and is shown for 2.1% Mn-doped sample. When Mn concentration is increased initially, more number of dopant centers would be available to facilitate better energy transfer from the host material to dopant states. However, further increase in Mn^{2+} concentration results in the interaction between neighboring Mn^{2+} dipoles essentially leading to luminescence quenching and decreases in PL intensity. Inset of figure 6b shows the photograph of 0 % and 0.9% Mn- doped $\text{Cs}_2\text{AgInCl}_6$ samples under a 254 nm UV illumination. Undoped sample shows a slight yellow color with very less intensity. This is in agreement with the PL data of undoped sample. On the other hand, Mn-doped sample shows a bright red color emission which agrees with the red PL emission of doped samples centered at 632 nm.

To find out the origin of this PL, PL decay measurements were conducted on both undoped and doped samples at a wavelength corresponding to their respective peak positions. The Mn-doped samples are expected to exhibit millisecond (ms) or sub-ms lifetimes since the ${}^4\text{T}_1 - {}^6\text{A}_1$ Mn d-d transitions are spin forbidden. Figure 6 shows the PL

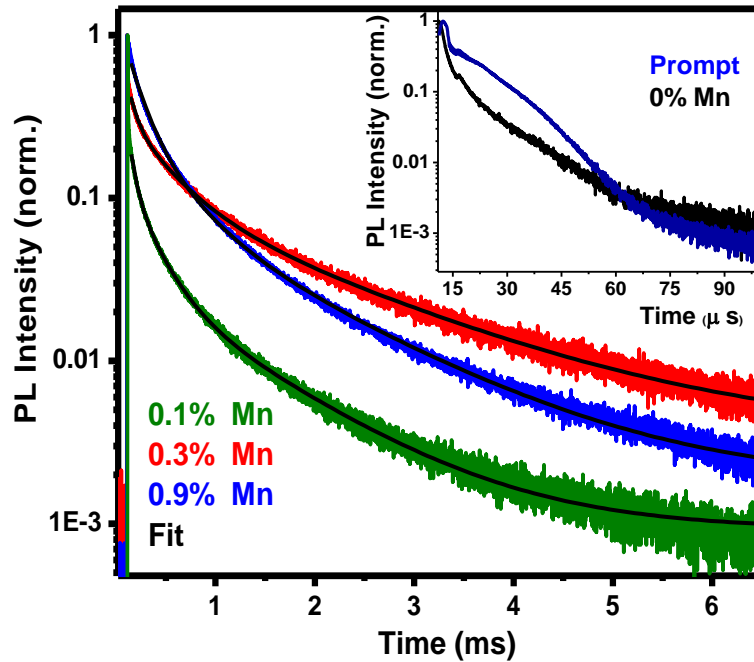


Figure 6: PL decay dynamics of 0.1%, 0.3% and 0.9% Mn-doped $\text{Cs}_2\text{AgInCl}_6$ samples collected at 632 nm with a 330 nm excitation. Inset figure shows the comparison of decay profile of 0% sample with instrument response function (prompt).

decay dynamics measured for all the doped samples, 0.1%, 0.3% and 0.9 %. They indeed show that PL lifetimes of doped samples are close to ms. Table 1 shows the fitting parameters and average lifetime of PL decays obtained for all doped samples. All decays are fitted using tri-exponential fit. An average lifetime of 367,974 and 595 microseconds (μs) were observed for 0.1, 0.3 and 0.9% Mn-doped samples respectively. Such long lifetime is accounted for the spin forbidden ${}^4\text{T}_1 - {}^6\text{A}_1$ transition of Mn d electrons and from isolated Mn^{2+} ions doped into $\text{Cs}_2\text{AgInCl}_6$ crystals¹⁹. The PL decay of undoped sample is similar to the instrument response function, as shown in the inset of figure 6. This is not surprising since the emission intensity of undoped sample is very poor. Volonakis et al.¹³ reported the PL lifetime of $\text{Cs}_2\text{AgInCl}_6$ consists of a fast and a slow component which when fitted individually by a mono exponential function yielded average lifetimes of 1 ns and 6 μs respectively. At the same time Zhou et al.¹⁶ reported a bi exponential fit with a fast (16.3 μs) and slow (100 μs) component. With a very small signal to noise ratio it is very difficult to accurately determine the PL lifetime of $\text{Cs}_2\text{AgInCl}_6$ double perovskites and this must be the reason for different lifetimes obtained by the above groups

Table 1: Fitting parameters and average lifetime of Mn-doped Cs₂AgInCl₆ double perovskite samples.

Sample (% Mn)	τ_1 (μs)	A1	τ_2 (μs)	A2	τ_3 (ms)	A3
0.1%	57.3	84.6 %	239	12.7 %	1.05	2.7 %
0.3%	76.1	70.6 %	398	21 %	1.67	8.4 %
0.9%	151	70.8 %	384	22.1 %	1.30	7.1 %

3.4 EPR studies

Figure 7 shows the X band EPR spectra recorded for 0.3% and 0.9% Mn-doped Cs₂AgInCl₆ halide double perovskite samples at room temperature. Both samples show a 6 fold hyperfine splitting structure corresponding to unpaired 3d electronic spin ($S=5/2$) and nuclear spin ($I=5/2$) of Mn²⁺ ions. The hyperfine splitting energy is found to be 8.7 mT (87 Gauss) and 8.5 mT (85 Gauss) for 0.3% and 0.9% Mn doped Cs₂AgInCl₆. These hyperfine splitting energies are similar to that reported for Mn-doped CsPbCl₃ nanoplatelets (8.6 mT)¹⁴. These sharp sextet hyperfine splitting lines confirm the presence of isolated Mn²⁺ ions in the lattice of Cs₂AgInCl₆ HDPs. As the Mn concentration is increased from 0.3% to 0.9% a small broadening in the EPR spectra is observed. This broadening is accounted by the exchange interactions between Mn dipoles as the concentration is increased. Thus the EPR spectra shown in figure 7 has two components; sharp hyperfine splitting corresponding to isolated Mn²⁺ ions within Cs₂AgInCl₆ lattice and another broad component arising from the Mn-Mn dipole interactions as Mn concentration is increased. The contribution of latter increases as Mn concentrations is increased further. At this point it is difficult to predict whether Mn²⁺ is substituting both Ag⁺ and In³⁺ by maintaining the charge neutrality or is there any preference for Mn²⁺ to any one of the site.

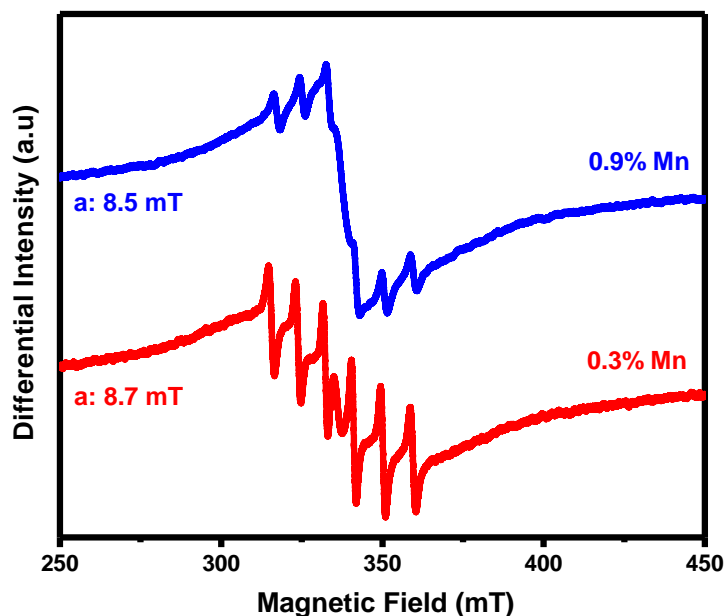


Figure 7: X band EPR spectra of 0.3% and 0.9% Mn-doped $\text{Cs}_2\text{AgInCl}_6$ measured at room-temperature. The spectra for 0.9% Mn is vertically shifted for a better view.

3.5 Stability studies

Oxide counterparts of double perovskites are said to have high crystalline stability owing to their rock-salt structure. Since halide double perovskites exhibits the same crystal structure, it is expected that they will also be structurally stable at ambient conditions. To understand the stability of undoped and doped $\text{Cs}_2\text{AgInCl}_6$ samples, they were stored in ambient atmosphere for 3 months. The XRD patterns given in figure 8a show no significant changes suggesting that even after 3 months undoped and doped $\text{Cs}_2\text{AgInCl}_6$ are structurally stable.

TGA curve for undoped and doped (0.3% and 0.69%) sample shown in figure 8b display similar weight loss characteristics. All samples are stable till a temperature of 525 °C which confirm their thermal stability. The data is recorded from 30 °C to 800 °C, though the weight loss is not complete at 800 °C. Since AgCl , MnCl_2 and CsCl has a high boiling point >1000 °C and InCl_3 boils at 800 °C, the weight loss is accounted for some secondary compound on decomposition of $\text{Cs}_2\text{AgInCl}_6$ after 525 °C. At 800 °C there is a 55% weight loss which can be due to the evaporation of CsInCl_4 . Thus by Figure 8 b), the decomposition of $\text{Cs}_2\text{AgInCl}_6$ at $T > 525$ °C can be written as $\text{Cs}_2\text{AgInCl}_6 - \text{CsInCl}_4 + \text{CsAgCl}_2$ which agrees with the report of Zhou et al¹⁶.

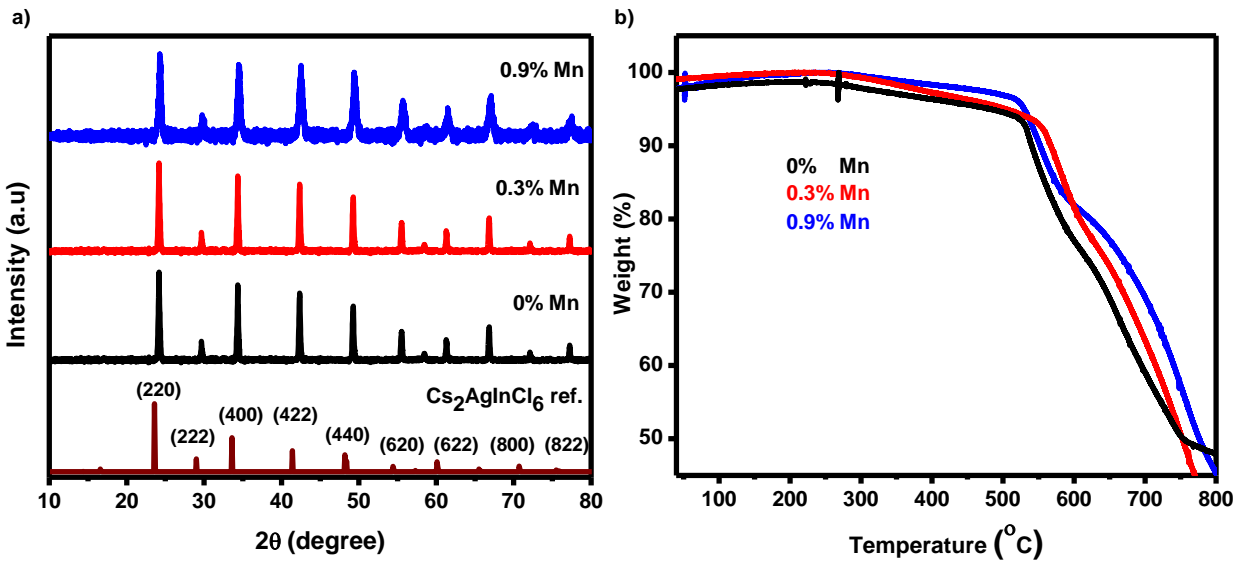


Figure 8: Powder XRD patterns of undoped (0%) and Mn-doped (0.3% and 0.9%) $\text{Cs}_2\text{AgInCl}_6$ samples after 3 months in ambient atmosphere. b) TGA curves of undoped (0%) and doped (0.3% and 0.9%) samples

4. Conclusion

In conclusion we successfully synthesized Mn-doped $\text{Cs}_2\text{AgInCl}_6$ halide double perovskites. XRD patterns showed no impurity peaks suggesting the formation of pure crystals. Also ICP-AES analysis showed <1% of Mn doping. Undoped and doped samples showed similar structural and morphological characteristics as well. A hyperfine splitting constant of 8.5 mT in EPR spectra confirms the incorporation of Mn^{2+} in to the crystal lattice. This Mn doping gives red color emission upon UV illumination. $\text{Cs}_2\text{AgInCl}_6$ with a band gap of ~ 3.5 eV absorbs this UV light and transfers the excitation energy to Mn d electrons. Subsequent de-excitation of Mn d electrons gives rise to a bright red emission with nearly millisecond long lifetime. Here doping has been employed to impart optical functionality to $\text{Cs}_2\text{AgInCl}_6$ HDP. Along with future attempts to achieve reasonably good charge transport, luminescent Mn-doped $\text{Cs}_2\text{AgInCl}_6$ can be used for making efficient light emitting diodes.

Part II

Attempts to dope lanthanide metal ions (Eu^{2+} and Sm^{3+}) into $\text{Cs}_2\text{AgInCl}_6$ halide double perovskite crystal

1. Introduction

Inorganic phosphor materials doped with divalent or trivalent lanthanide dopants are known to exhibit interesting optical properties like bright and sharp band emission, increased photoluminescence lifetime and a tunable emission in visible to near infrared (IR) region upon UV excitation^{21 22}. Moreover all lanthanide ions exhibit high chemical and photochemical stability with less toxicity²³. All these interesting properties have enabled lanthanide doped materials to be widely used for different technological purposes like LED's, sensors, lasers, fluorescent lamps and electroluminescent devices²⁴.

The unique properties of lanthanide ions arise due to their 4f electronic configuration. Moving from Lanthanum (La) to Lutetium (Lu) in the series, gradual filling of 4f orbital takes place. The luminescence properties of lanthanide doped materials can be considered as a result of intra f-f transition or 4f-5d transitions of lanthanide ions upon energy transfer from host. Due to poor shielding, partly filled 4f orbitals penetrate into $5s^2$ and $5p^6$ core orbitals of xenon core. This restrict the ligands (in the host) to cause any small amount of perturbation to 4f orbitals. This phenomenon known as lanthanide contraction is the reason for the sharp emission and long lifetime observed for lanthanide ion doped systems.

Out of all lanthanide elements, Europium (Eu^{2+} or Eu^{3+}) doped materials became an extensively studied system because of their ability to tune emission in visible region²⁵. For example certain Eu^{2+} doped chloride system emits in the violet region where as some bromide systems emits in blue region²⁵. These emissions are due to a parity allowed transition from $4f^65d^1$ to $4f^7$ state of Eu dopants. This variability in emission wavelength is caused by the environment of doped Eu ions; the crystal field splitting, coordination number, Eu-anionic ligand bond length and covalence²⁶. In a recent report

by Pan et al.²⁷, Eu³⁺ doped CsPbCl₃ nanocrystals showed sharp emissions at orange-red region of visible spectrum. They also reported yellow emission for Samarium (Sm³⁺) doped in the same perovskite system. Sm is also a well studied system as Eu and is known for its orange emission upon doping in bulk materials. From all the above examples it is clear that the emission from doped Eu and Sm ions depends majorly on the systems to which they are doped.

As already discussed in part I, Mn²⁺ doped Cs₂AgInCl₆ halide double perovskites has a broad emission centered in the red region, because of the spin forbidden ⁴T₁ – ⁶A₁ d-d transitions of Mn²⁺ electrons. The major drawback of such emissions is they cover only a specific wavelength range and are limited to it. For a system like Cs₂AgInCl₆, halide ion exchange is not possible since its bromide or iodide counterparts does not exists due to the less stability of MX₆ octahedra (M – Ag⁺, In³⁺; X- Br⁻, I⁻)¹³. So it is of great importance to bring multi color emission in Cs₂AgInCl₆ halide double perovskites by tailoring its optical emission properties by suitable band gap engineering.

In this regard doping lanthanide metal ions into Cs₂AgInCl₆ appear as a novel and promising method to impart multi color emission into the system along with Mn²⁺ ions. Moreover certain lanthanide doping has shown to increase the excitonic emission in lead halide perovskite system as reported by Pan et al.²⁷ in spite of the excitonic energy transfer from host CsPbCl₃ to lanthanide dopant ions. The reason for such a parallel enhancement of excitonic as well as dopant emission is said to be due to the removal or change of certain defect states in host material by dopant ions. Thus doping of lanthanide ions, especially Eu²⁺ or Sm³⁺ seems to be a promising way to enhance the existing emission properties of Cs₂AgInCl₆ in the visible region. Achieving dopant related emission in the blue-violet region can lead to the development of stable and sharp emitter materials for LEDs. Also this lanthanide doping can be extended to Mn-doped Cs₂AgInCl₆ for generating multi color emission from the double perovskite material. This would open a new way for developing stable and highly emissive multicolor LED's using a single material in future instead of using multicolor phosphor composites.

2. Methodology

2.1 Materials

Hydrochloric acid (HCl, Purity-37 wt %), Cesium chloride (CsCl, 99.9%), Indium trichloride (InCl₃, Anhydrous powder, 99.999%), Silver chloride (AgCl, 99.999%), Europium (II) chloride (EuCl₂, 99.99%) and Samarium (III) nitrate hexahydrate (Sm(NO₃)₃.6H₂O, 99.999%) were purchased from Sigma Aldrich Chemicals. Ethanol (>99.9%) and Acetone (>99.9%) were purchased from Rankem chemicals. All the precursors were used as received without further purifications

2.2 Synthesis

Undoped and Eu²⁺ or Sm³⁺ doped Cs₂AgInCl₆ was synthesized by acid precipitation synthesis protocol that has been described in part I with slight modifications¹³. For undoped sample, 0.5 mmol of AgCl and InCl₃ each were taken in 3 ml 10M HCl. The vial containing the above precursors was kept heating at 72 °C under vigorous stirring. Later on 1 mmol of CsCl was added under stirring, forming a pale white precipitate immediately. The mixture was kept heating for another 20 min to ensure complete reaction of all the precursors. Afterwards the precipitate was filtered, washed with ethanol and dried in oven at 100 °C overnight. For doping 5% of Eu²⁺ and Sm³⁺, 0.05 mmol of EuCl₂ and Sm(NO₃)₃.6H₂O each were taken along with rest of the precursors in independent vials. The synthesizing protocol was similar as described above.

2.3 Instrumental Characterization

Powder XRD measurements were carried out in a 2 θ range of 10° to 60° using a Bruker D8 Advanced X-ray Diffractometer equipped with Cu K α radiation of wavelength 1.54 Å. All solid samples were grounded into fine powder for before analysis. The measurements were done on a glass substrate at a scan speed of 0.1. UV- Visible diffuse reflectance spectroscopy is carried out by Shimadzu UV 3000 600Plus UV-Vis/NIR Spectrophotometer in the range of 200 nm- 800 nm. This data is converted to absorption using Kubelka–Munk function³¹. All PL measurements were carried out using

FLS980 fluorescence spectrometer, Edinburg Instruments at an excitation wavelength of 330 nm.

3. Results and Discussion

3.1: Structural Characterization

The concentrations of Eu and Sm dopants correspond to their precursor concentration taken during synthesis. XRD patterns of undoped (0%) and doped (5% Eu^{2+} and 5% Sm^{3+}) given in Figure 9 clearly agrees with the reference data of $\text{Cs}_2\text{AgInCl}_6$. No additional peaks are observed in the XRD patterns of any samples suggesting the absence of Eu or Sm related impurities. The Shannon radii of Eu^{2+} and Sm^{3+} in an octahedral environment is 1.17 \AA and 0.96 \AA respectively, which is relatable to Ag^+ (1.15 \AA) and In^{3+} (0.8 \AA) in the same conditions. Hence, doping Eu^{2+} or Sm^{3+} into $\text{Cs}_2\text{AgInCl}_6$ crystal is expected to replace either Ag^+ or In^{3+} or both from their respective octahedra. This may or may not create a 2θ shift in XRD pattern. However, the XRD peaks of doped samples show no 2θ shift compared to undoped sample. At this point it is not possible to conclude whether lanthanide ions are doped into HDP crystal lattice or

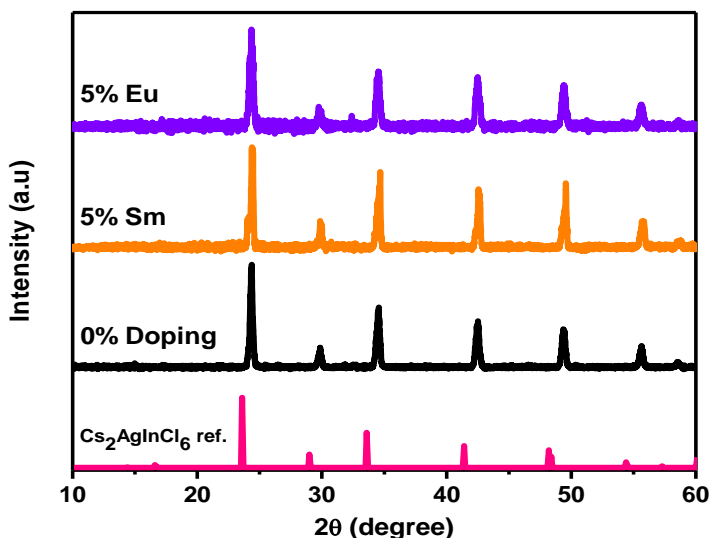


Figure 9: Powder XRD pattern for undoped (0%) and Eu^{2+} and Sm^{3+} doped $\text{Cs}_2\text{AgInCl}_6$ samples. All data are vertically shifted for a better view. Dopant concentration given is that of added precursors.

or not. Further experimental evidences (example, X-ray Photoelectron Spectroscopy (XPS) or ICP-AES) are required for confirming doping.

3.2 Optical Characterization

Figure 10a shows the UV visible spectra for undoped and Eu^{2+} and Sm^{3+} doped samples. The absorption onset of Eu^{2+} -doped and Sm^{3+} -doped $\text{Cs}_2\text{AgInCl}_6$ is at 350 nm (3.5 eV) which overlap with the undoped sample band gap. This suggests that there is no band gap change in the doped sample from the undoped samples. This suggests either the doping is unsuccessful or the amount of dopants incorporated is very less so as to give a pronounced shift in UV data, which is the usual observation for lanthanide doping. Pan et al.²⁷ recently reported that by lanthanide doping band gap of CsPbCl_3 nanocrystals increases due to lattice contraction created by incorporated dopants. We do not observe such changes in lanthanide doped $\text{Cs}_2\text{AgInCl}_6$ because of bulk nature of host in comparison with the nano regime samples.

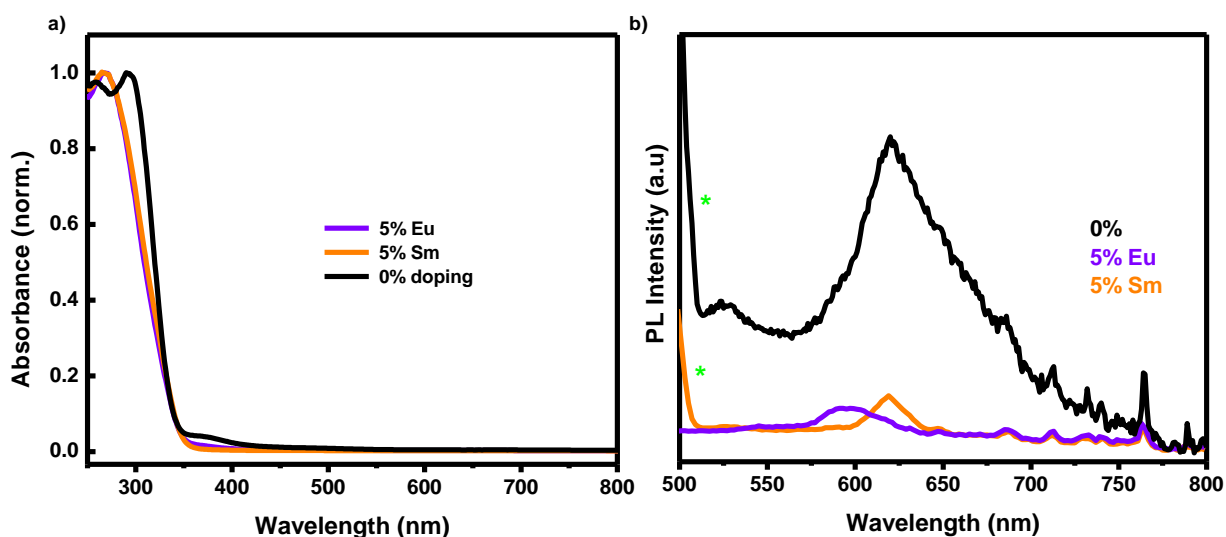


Figure 10 a) UV- Vis spectra of undoped and lanthanide doped samples. b) Steady state PL spectra of undoped and lanthanide doped samples (λ_{exc} : 330 nm) Green asterisks indicates scattering peaks.

To further confirm about the incorporation of lanthanide ions (Eu^{2+} and Sm^{3+}), PL studies were performed on the doped samples. In contrary to the expected emission by Eu^{2+} or Sm^{3+} doped samples, the PL of all doped samples got quenched compared to

undoped samples. This suggests that Eu^{2+} or Sm^{3+} might have doped inside $\text{Cs}_2\text{AgInCl}_6$ crystals but their effect observed is in contradiction to the expected results. One possible reason can be due to dopant band gap being higher to host band gap. Emission from Lanthanide dopants happen due to an electronic energy transfer from the host upon excitation. In such a scenario, efficient energy transfer is difficult to happen from host to dopant and PL can get quenched. Observing PL quenching in host material does not necessarily mean that doping could have happen. This can happen due to different reasons apart from doping.

4. Conclusion

Synthesis of lanthanide ion (Eu^{2+} or Sm^{3+}) doped $\text{Cs}_2\text{AgInCl}_6$ HDP was carried out and characterized by XRD, UV-Vis spectroscopy and steady state PL measurements. XRD and UV data for doped and undoped samples were similar. XRD peaks of doped samples showed no 2θ shift compared to undoped samples. However the PL of all doped samples got quenched. At this point it is very difficult to confirm doping in $\text{Cs}_2\text{AgInCl}_6$ HDP crystals. More experimental analysis like EDX, ICP-AES etc. would be able to give information about the doped lanthanide concentration, if any.

Part III

Attempt to synthesize $\text{Cs}_2\text{AgIn}(\text{Cl}/\text{Br})_6$ mix halide double perovskite

1. Introduction

Metal halide double perovskites (HDP's) with a general formula $\text{A}_2\text{B}^{\text{I}}\text{C}^{\text{III}}\text{X}_6$ (A- Cs^+ , B^{I} - Ag^+ , Cu^+ C^{III} - Bi^{3+} , In^{3+} X- Cl^- , Br^- , I^-) have been reported as a promising class of material for PV application and a possible future alternative for organic- inorganic hybrid lead halide perovskites owing to their inherent stability and Pb-free nature¹⁰. Most of such HDP's are predicted to have tunable band gaps in visible as well as near infrared region for better harvesting of solar energy and low effective charge carrier masses which aid in charge extraction and transport in a solar cell^{10 28 29}. However, many such HDPs exist only as per theoretical calculations and much experimental reports are not published yet. Recently, Bi^{3+} based HDP $\text{Cs}_2\text{AgBiBr}_6$ with a band gap ~ 1.95 eV was reported with a long PL lifetime of ~ 660 ns, defect tolerant nature and low carrier effective masses which are ideal for light absorbing materials in solar cells³⁰. But these materials have an indirect band gap that limits their PV application³⁰.

$\text{Cs}_2\text{AgInCl}_6$ HDP with inherent stability, direct band gap and low carrier effective masses ($m_{e}^* 0.32m_0$ and $m_{\text{h}}^* 0.43m_0$) have favorable features for PV application^{13 10}. However this material has a wide band gap (3.5 eV) which absorbs in the near UV region making them unsuitable for solar cell devices. The bromide or iodide counterparts of this material namely $\text{Cs}_2\text{AgInBr}_6$ and $\text{Cs}_2\text{AgInI}_6$ have a band gap tunable in the visible and infrared region (1.7 eV and 0.5 eV respectively)¹⁰. But computational studies on these systems predicted thermodynamic instability of $\text{Cs}_2\text{AgInI}_6$ compared to $\text{Cs}_2\text{AgInBr}_6$. $\text{Cs}_2\text{AgInBr}_6$ has low charge carrier effective masses ($m_{e}^* 0.24m_0$ and $m_{\text{h}}^* 0.34m_0$), thermodynamic stability and a narrow and direct band gap^{13 10}. To understand more about the material stability using Goldschmidt's stability criteria, Volonakis et al.¹³ calculated the tolerance factor (t) and octahedral factor (μ) for $\text{Cs}_2\text{AgInBr}_6$. Even though they showed a normal t and μ ($0.75 < t < 1.0$; $\mu > 0.41$) initially, further detailed study

showed a lower μ than the normal value and consequent inability of these materials to form a stable 3D structure. These values are shown in figure 11 where the octahedral factor is favorable for only $\text{Cs}_2\text{AgInCl}_6$ and $\text{Cs}_2\text{AgIn}(\text{Cl}/\text{Br})_6$ HDP's. Thus other than $\text{Cs}_2\text{AgInCl}_6$, the only material among $\text{Ag}^+/\text{In}^{3+}$ based HDP's that are structurally stable and could be synthesized is $\text{Cs}_2\text{AgIn}(\text{Cl}/\text{Br})_6$.

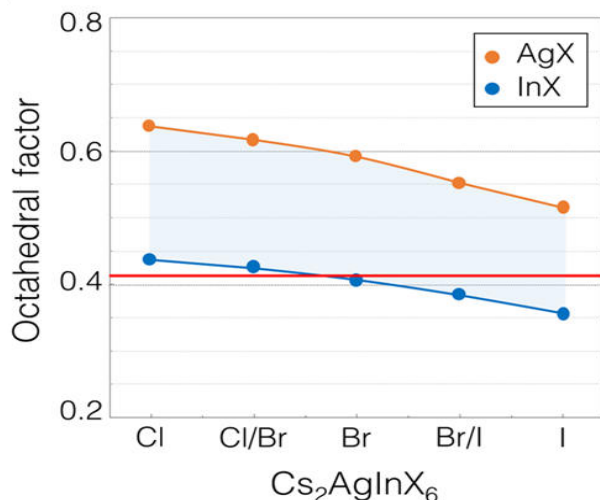


Figure 11: Octahedral factor calculated for $\text{Cs}_2\text{AgInX}_6$ (X- Cl, Cl/Br, Br, Br/I). Figure adapted with permission from Volonakis et al¹³. Copyright 2017, American Chemical Society

In this part, we attempt to synthesize $\text{Cs}_2\text{AgIn}(\text{Cl}/\text{Br})_6$ mix halide double perovskite and characterize the sample with XRD and UV-visible spectroscopy. This material is expected to have a band gap in between 3.5 eV ($\text{Cs}_2\text{AgInCl}_6$) and 1.7 eV ($\text{Cs}_2\text{AgInBr}_6$) and by changing the Cl: Br ratio desired band gap could be achieved. Thus the aim of Part III is to successfully synthesize $\text{Cs}_2\text{AgIn}(\text{Cl}/\text{Br})_6$ for future solar device applications.

2. Methodology

2.1 Materials

Hydrobromic acid (HBr, Purity-48 wt%), Cesium chloride (CsCl, 99.9%), Indium trichloride (InCl_3 , Anhydrous powder, 99.999%), Silver chloride (AgCl, 99.999%) were purchased from Sigma Aldrich Chemicals. Ethanol (>99.9%) and Acetone (>99.9%)

were purchased from Rankem chemicals. All the precursors were used as received without further purifications.

2.2 Synthesis

To prepare $\text{Cs}_2\text{AgIn}(\text{Cl}/\text{Br})_6$ mix HDPs, 0.5 mmol of AgCl and InCl_3 each were taken in 5 ml HBr. The vial containing the above precursors was kept heating at 115 °C under vigorous stirring until all the precursors dissolve. Later on 1 mmol of CsCl was added under stirring. The solution remained colorless and clear. The mixture was kept heating for another 20 min to ensure complete reaction of all the precursors. Afterwards the solution was allowed to cool to room temperature slowly forming white and shiny crystals. The crystals were filtered, washed with ethanol and dried in oven at 100 °C overnight.

2.3 Instrumental Characterization

Powder XRD measurements were carried out in a 2θ range of 10° to 60° using a Bruker D8 Advanced X-ray Diffractometer equipped with Cu $K\alpha$ radiation of wavelength 1.54 Å. Samples were grounded into fine powder before analysis. The measurements were done on a glass substrate at a scan speed of 0.1. UV- Visible diffuse reflectance spectroscopy is carried out by Shimadzu UV 3000 600Plus UV-Vis/NIR Spectrophotometer in the range of 200 nm-800 nm. This data is converted to absorption using Kubelka –Munk function³¹.

3. Results and Discussion

3.1 Structural analysis

XRD pattern recorded for the as prepared $\text{Cs}_2\text{AgIn}(\text{Cl}/\text{Br})_6$ is displayed in figure 12 along with $\text{Cs}_2\text{AgInCl}_6$ reference data¹³. It shows the peaks corresponding to reference pattern suggesting the formation of $\text{Cs}_2\text{AgInCl}_6$. However the peak intensities are different from the reference data and are overlapped by many impurity peaks. Since the synthesis is carried out in an open vessel, there is a chance of forming oxide impurity along with the desired product. The octahedral factor for Cl/Br mix HDP is close to the

threshold value compared to $\text{Cs}_2\text{AgInCl}_6$. Hence the crystal formation will be difficult and slow, causing other impurity pathways competing to overtake the Cl/Br mix HDP formation. Synthesis is carried out 115 °C and cannot be raised beyond 120 °C since

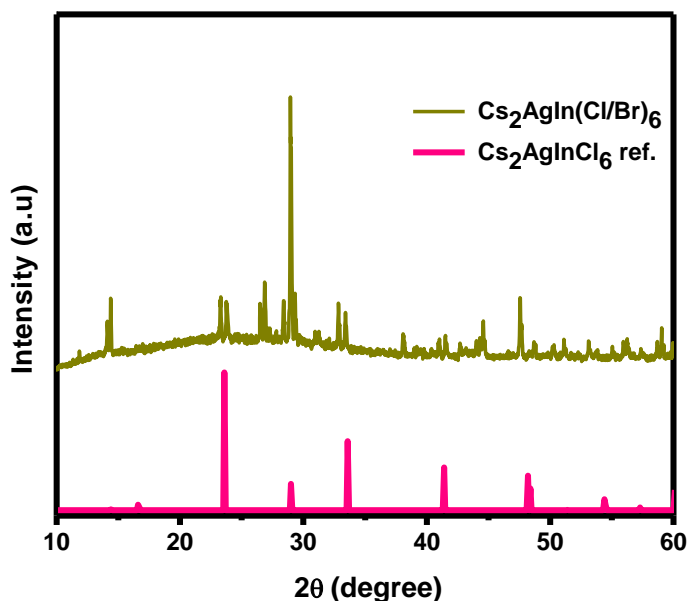


Figure 12: Powder XRD pattern of as synthesized $\text{Cs}_2\text{AgIn(Cl/Br)}_6$ mix halide double perovskite

the boiling point of HBr is 122 °C. If the synthesis would have carried out at elevated temperature, there is a possibility of the product formation with little side products. The use of other Br precursor's were also tried in HCl, but was not successful either.

3.2 Optical Characterization

UV –Vis absorption spectra collected for as prepared $\text{Cs}_2\text{AgIn(Cl/Br)}_6$ mix HDP is given in figure 13. This is similar to the absorption data for $\text{Cs}_2\text{AgInCl}_6$ given in the same figure. But the absorption onset is shifted from 350 nm (3.5 eV) to 333 nm (3.7 eV). This might be due to measurement errors. The color of the compound appears white similar to $\text{Cs}_2\text{AgInCl}_6$ under ambient light. Thus optical analyses suggest the formation of $\text{Cs}_2\text{AgInCl}_6$ instead of a Cl/Br mix of the same material. This must be due to the ease in formation of $\text{Cs}_2\text{AgInCl}_6$ compared to $\text{Cs}_2\text{AgIn(Cl/Br)}_6$.

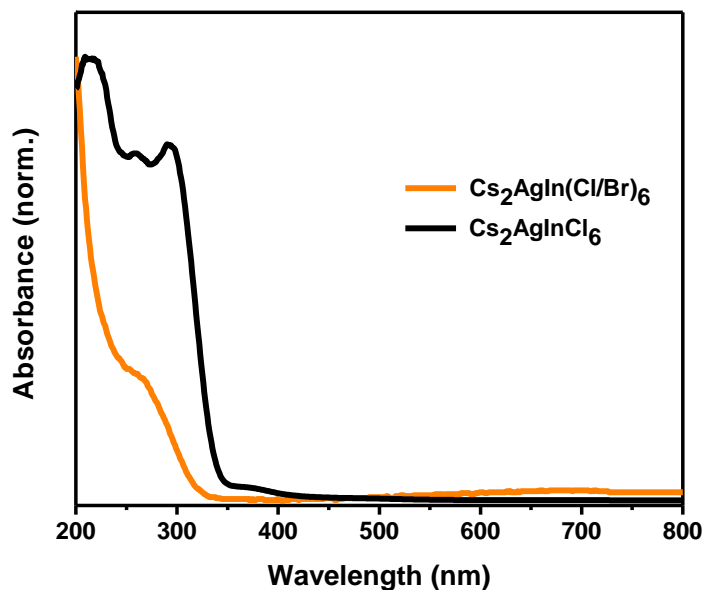


Figure 13: UV-Visible absorption spectra of as prepared $\text{Cs}_2\text{AgIn}(\text{Cl}/\text{Br})_6$ HDPs

4. Conclusion

Synthesis of $\text{Cs}_2\text{AgIn}(\text{Cl}/\text{Br})_6$ mix halide double perovskite was unsuccessful. Structural and optical characterization of as prepared samples showed the formation of $\text{Cs}_2\text{AgInCl}_6$ instead of Cl/Br mix. This might be due to comparatively low formation energy of $\text{Cs}_2\text{AgInCl}_6$ compared to Cl/Br mix HDPs. A revised experimental strategy should be adopted for the synthesis of Cl/Br mix of $\text{Ag}^+/\text{In}^{3+}$ HDPs. This can only be achieved by a detailed understanding of the formation mechanism of the same.

References

- (1) Burschka, J.; Pellet, N.; Moon, S.-J.; Humphry-Baker, R.; Gao, P.; Nazeeruddin, M. K.; Grätzel, M. Sequential Deposition as a Route to High-Performance Perovskite-Sensitized Solar Cells. *Nature* **2013**, *499*, 316–319.
- (2) Kojima, A.; Teshima, K.; Shirai, Y.; Miyasaka, T. Organometal Halide Perovskites as Visible-Light Sensitizers for Photovoltaic Cells. *J. Am. Chem. Soc.* **2009**, *131*, 6050–6051.
- (3) Akbulatov, A. F.; Luchkin, S. Y.; Frolova, L. A.; Dremova, N. N.; Gerasimov, K. L.; Zhidkov, I. S.; Anokhin, D. V.; Kurmaev, E. Z.; Stevenson, K. J.; Troshin, P. A. Probing the Intrinsic Thermal and Photochemical Stability of Hybrid and Inorganic Lead Halide Perovskites. *J. Phys. Chem. Lett.* **2017**, *8*, 1211–1218.
- (4) Kovalenko, M. V.; Protesescu, L.; Bodnarchuk, M. I. Properties and Potential Optoelectronic Applications of Lead Halide Perovskite Nanocrystals. **2017**, *750*, 745–750.
- (5) Conings, B.; Drijkoningen, J.; Gauquelin, N.; Babayigit, A.; D'Haen, J.; D'Olieslaeger, L.; Ethirajan, A.; Verbeeck, J.; Manca, J.; Mosconi, E.; et al. Intrinsic Thermal Instability of Methylammonium Lead Trihalide Perovskite. *Adv. Energy Mater.* **2015**, *5*, 1500477.
- (6) Swarnkar, A.; Marshall, A. R.; Sanehira, E. M.; Chernomordik, B. D.; Moore, D. T.; Christians, J. A.; Chakrabarti, T.; Luther, J. M. Quantum Dot-Induced Phase Stabilization of -CsPbI₃ Perovskite for High-Efficiency Photovoltaics. *Science* (80- .). **2016**, *354*, 92–95.
- (7) Ravi, V. K.; Markad, G. B.; Nag, A. Band Edge Energies and Excitonic Transition Probabilities of Colloidal CsPbX₃ (X = Cl, Br, I) Perovskite Nanocrystals. *ACS Energy Lett.* **2016**, *1*, 665–671.
- (8) Swarnkar, A.; Ravi, V. K.; Nag, A. Beyond Colloidal Cesium Lead Halide Perovskite Nanocrystals: Analogous Metal Halides and Doping. *ACS Energy Lett.* **2017**, *2*, 1089–1098.
- (9) Lyu, M.; Yun, J. H.; Chen, P.; Hao, M.; Wang, L. Addressing Toxicity of Lead: Progress and Applications of Low-Toxic Metal Halide Perovskites and Their Derivatives. *Adv. Energy Mater.* **2017**, *7*.
- (10) Zhao, X. G.; Yang, D.; Sun, Y.; Li, T.; Zhang, L.; Yu, L.; Zunger, A. Cu-In Halide Perovskite Solar Absorbers. *J. Am. Chem. Soc.* **2017**, *139*, 6718–6725.
- (11) Zhao, X. G.; Yang, J. H.; Fu, Y.; Yang, D.; Xu, Q.; Yu, L.; Wei, S. H.; Zhang, L. Design of Lead-Free Inorganic Halide Perovskites for Solar Cells via Cation-Transmutation. *J. Am. Chem. Soc.* **2017**, *139*, 2630–2638.
- (12) McClure, E. T.; Ball, M. R.; Windl, W.; Woodward, P. M. Cs₂AgBiX₆ (X = Br, Cl): New Visible Light Absorbing, Lead-Free Halide Perovskite Semiconductors. *Chem. Mater.* **2016**, *28*, 1348–1354.
- (13) Volonakis, G.; Haghighirad, A. A.; Milot, R. L.; Sio, W. H.; Filip, M. R.; Wenger, B.; Johnston, M. B.; Herz, L. M.; Snaith, H. J.; Giustino, F. Cs₂InAgCl₆: A New Lead-Free Halide Double Perovskite with Direct Band Gap. *J. Phys. Chem. Lett.* **2017**, *8*, 772–778.

- (14) Mir, W. J.; Jagadeeswararao, M.; Das, S.; Nag, A. Colloidal Mn-Doped Cesium Lead Halide Perovskite Nanoplatelets. *ACS Energy Lett.* **2017**, *2*, 537–543.
- (15) Tran, T. T.; Panella, J. R.; Chamorro, J. R.; Morey, J. R.; McQueen, T. M. Designing Indirect–direct Bandgap Transitions in Double Perovskites. *Mater. Horiz.* **2017**, *4*, 688–693.
- (16) Zhou, J.; Xia, Z.; Molocheev, M. S.; Zhang, X.; Peng, D.; Liu, Q. Composition Design, Optical Gap and Stability Investigations of Lead-Free Halide Double Perovskite Cs₂AgInCl₆. *J. Mater. Chem. A* **2017**, *5*, 15031–15037.
- (17) Lin, J.; Hu, D. D.; Zhang, Q.; Li, D. S.; Wu, T.; Bu, X.; Feng, P. Improving Photoluminescence Emission Efficiency of Nanocluster-Based Materials by in Situ Doping Synthetic Strategy. *J. Phys. Chem. C* **2016**, *120*, 29390–29396.
- (18) Beaulac, R.; Archer, P. I.; Ochsenein, S. T.; Gamelin, D. R. Mn²⁺-Doped CdSe Quantum Dots: New Inorganic Materials for Spin-Electronics and Spin-Photonics. *Adv. Funct. Mater.* **2008**, *18*, 3873–3891.
- (19) Guria, A. K.; Dutta, S. K.; Adhikari, S. Das; Pradhan, N. Doping Mn²⁺ in Lead Halide Perovskite Nanocrystals: Successes and Challenges. *ACS Energy Lett.* **2017**, *2*, 1014–1021.
- (20) Nag, A.; Sapra, S.; Nagamani, C.; Sharma, A.; Pradhan, N.; Bhat, S. V.; Sarma, D. D. A Study of Mn²⁺ Doping in CdS Nanocrystals. *Chem. Mater.* **2007**, *19*, 3252–3259.
- (21) Ewa M. Goldys, *, †; Krystyna Drozdowicz-Tomsia, †; Sun Jinjun, †; Dosi Dosev, ‡; Ian M. Kennedy, ‡; Sergiy Yatsunencko, § and; Godlewski§, M. Optical Characterization of Eu-Doped and Undoped Gd₂O₃ Nanoparticles Synthesized by the Hydrogen Flame Pyrolysis Method. *J. Am. Chem. Soc.* **2006**, *128*, 14498–14505.
- (22) Gordon, W. O.; Carter, J. A.; Tissue, B. M. Long-Lifetime Luminescence of Lanthanide-Doped Gadolinium Oxide Nanoparticles for Immunoassays. *J. Lumin.* **2004**, *108*, 339–342.
- (23) Cheng, L.; Yang, K.; Li, Y.; Chen, J.; Wang, C.; Shao, M.; Lee, S.-T.; Liu, Z. Facile Preparation of Multifunctional Upconversion Nanoprobes for Multimodal Imaging and Dual-Targeted Photothermal Therapy. *Angew. Chemie Int. Ed.* **2011**, *50*, 7385–7390.
- (24) Höpfe, H. A. Recent Developments in the Field of Inorganic Phosphors. *Angew. Chemie Int. Ed.* **2009**, *48*, 3572–3582.
- (25) Terraschke, H.; Wickleder, C. UV, Blue, Green, Yellow, Red, and Small: Newest Developments on Eu²⁺-Doped Nanophosphors. *Chem. Rev.* **2015**, *115*, 11352–11378.
- (26) Zhou, B.; Tao, L.; Chai, Y.; Lau, S. P.; Zhang, Q.; Tsang, Y. H. Constructing Interfacial Energy Transfer for Photon Up- and Down-Conversion from Lanthanides in a Core–Shell Nanostructure. *Angew. Chemie - Int. Ed.* **2016**, *55*, 12356–12360.
- (27) Pan, G.; Bai, X.; Yang, D.; Chen, X.; Jing, P.; Qu, S.; Zhang, L.; Zhou, D.; Zhu, J.; Xu, W.; et al. Doping Lanthanide into Perovskite Nanocrystals: Highly Improved and Expanded Optical Properties. *Nano Lett.* **2017**, *17*, 8005–8011.
- (28) Feng, H.-J.; Deng, W.; Yang, K.; Huang, J.; Zeng, X. C. Double Perovskite Cs₂BBiX₆ (B = Ag, Cu; X = Br, Cl)/TiO₂ Heterojunction: An Efficient Pb-Free

- Perovskite Interface for Charge Extraction. *J. Phys. Chem. C* **2017**, *121*, 4471–4480.
- (29) Slavney, A. H.; Leppert, L.; Bartesaghi, D.; Gold-Parker, A.; Toney, M. F.; Savenije, T. J.; Neaton, J. B.; Karunadasa, H. I. Defect-Induced Band-Edge Reconstruction of a Bismuth-Halide Double Perovskite for Visible-Light Absorption. *J. Am. Chem. Soc.* **2017**, *139*, 5015–5018.
- (30) Slavney, A. H.; Hu, T.; Lindenberg, A. M.; Karunadasa, H. I. A Bismuth-Halide Double Perovskite with Long Carrier Recombination Lifetime for Photovoltaic Applications. *J. Am. Chem. Soc.* **2016**, *138*, 2138–2141.
- (31) P. Kubelka and F. Munk, *Z. Techn. Phys.*, 1931, *12*, 593–601.

**RightsLink**®[Home](#)[Create Account](#)[Help](#)

Title: Cu-In Halide Perovskite Solar Absorbers

Author: Xin-Gang Zhao, Dongwen Yang, Yuanhui Sun, et al

Publication: Journal of the American Chemical Society

Publisher: American Chemical Society

Date: May 1, 2017

Copyright © 2017, American Chemical Society

LOGIN

If you're a **copyright.com user**, you can login to RightsLink using your copyright.com credentials.

Already a **RightsLink user** or want to [learn more?](#)

PERMISSION/LICENSE IS GRANTED FOR YOUR ORDER AT NO CHARGE

This type of permission/license, instead of the standard Terms & Conditions, is sent to you because no fee is being charged for your order. Please note the following:

- Permission is granted for your request in both print and electronic formats, and translations.
- If figures and/or tables were requested, they may be adapted or used in part.
- Please print this page for your records and send a copy of it to your publisher/graduate school.
- Appropriate credit for the requested material should be given as follows: "Reprinted (adapted) with permission from (COMPLETE REFERENCE CITATION). Copyright (YEAR) American Chemical Society." Insert appropriate information in place of the capitalized words.
- One-time permission is granted only for the use specified in your request. No additional uses are granted (such as derivative works or other editions). For any other uses, please submit a new request.

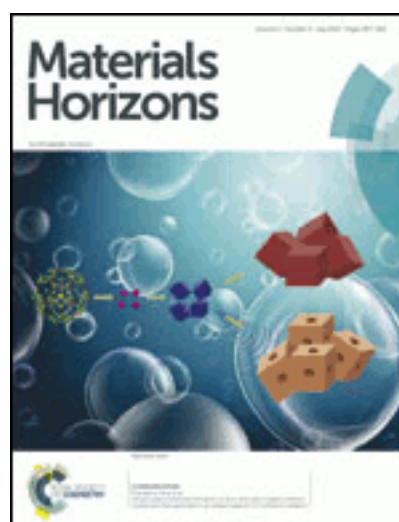
If credit is given to another source for the material you requested, permission must be obtained from that source.

[BACK](#)[CLOSE WINDOW](#)

Copyright © 2018 [Copyright Clearance Center, Inc.](#) All Rights Reserved. [Privacy statement.](#) [Terms and Conditions.](#)
Comments? We would like to hear from you. E-mail us at customercare@copyright.com



RightsLink®

[Home](#)
[Account Info](#)
[Help](#)


Title: Designing indirect–direct bandgap transitions in double perovskites

Author: T. Thao Tran, Jessica R. Panella, Juan R. Chamorro, Jennifer R. Morey, Tyrel M. McQueen

Publication: Materials Horizons

Publisher: Royal Society of Chemistry

Date: Jun 1, 2017

Copyright © 2017, Royal Society of Chemistry

Logged in as:

Nila Nandha K

[LOGOUT](#)

Order Completed

Thank you for your order.

This Agreement between Ms. Nila Nandha K ("You") and Royal Society of Chemistry ("Royal Society of Chemistry") consists of your license details and the terms and conditions provided by Royal Society of Chemistry and Copyright Clearance Center.

Your confirmation email will contain your order number for future reference.

[printable details](#)

License Number	4335910465283
License date	Apr 25, 2018
Licensed Content Publisher	Royal Society of Chemistry
Licensed Content Publication	Materials Horizons
Licensed Content Title	Designing indirect–direct bandgap transitions in double perovskites
Licensed Content Author	T. Thao Tran, Jessica R. Panella, Juan R. Chamorro, Jennifer R. Morey, Tyrel M. McQueen
Licensed Content Date	Jun 1, 2017
Licensed Content Volume	4
Licensed Content Issue	4
Type of Use	Thesis/Dissertation
Requestor type	non-commercial (non-profit)
Portion	figures/tables/images
Number of figures/tables /images	1
Distribution quantity	100
Format	print and electronic
Will you be translating?	no
Order reference number	
Title of the thesis/dissertation	Doping metal ions into Cs ₂ AgInCl ₆ halide double perovskites
Expected completion date	May 2018
Estimated size	43
Attachment	

Requestor Location Ms. Nila Nandha K
New hostel 1, IISER campus, IISER,
Dr. Homi Bhabaha Road, Pashan, pune

Pune, Maarastra state 411008
India
Attn: Ms. Nila Nandha K

Billing Type Invoice

Billing address Ms. Nila Nandha K
New hostel 1, IISER campus, IISER,
Dr. Homi Bhabaha Road, Pashan, pune

Pune, India 411008
Attn: Ms. Nila Nandha K

Total 0.00 USD

ORDER MORE

CLOSE WINDOW

Copyright © 2018 [Copyright Clearance Center, Inc.](#) All Rights Reserved. [Privacy statement.](#) [Terms and Conditions.](#)
Comments? We would like to hear from you. E-mail us at customercare@copyright.com



RightsLink®

[Home](#)[Create Account](#)[Help](#)

Title: Cs₂InAgCl₆: A New Lead-Free Halide Double Perovskite with Direct Band Gap

Author: George Volonakis, Amir Abbas Haghighirad, Rebecca L. Milot, et al

Publication: Journal of Physical Chemistry Letters

Publisher: American Chemical Society

Date: Feb 1, 2017

Copyright © 2017, American Chemical Society

LOGIN

If you're a **copyright.com user**, you can login to RightsLink using your copyright.com credentials.

Already a **RightsLink user** or want to [learn more?](#)

PERMISSION/LICENSE IS GRANTED FOR YOUR ORDER AT NO CHARGE

This type of permission/license, instead of the standard Terms & Conditions, is sent to you because no fee is being charged for your order. Please note the following:

- Permission is granted for your request in both print and electronic formats, and translations.
- If figures and/or tables were requested, they may be adapted or used in part.
- Please print this page for your records and send a copy of it to your publisher/graduate school.
- Appropriate credit for the requested material should be given as follows: "Reprinted (adapted) with permission from (COMPLETE REFERENCE CITATION). Copyright (YEAR) American Chemical Society." Insert appropriate information in place of the capitalized words.
- One-time permission is granted only for the use specified in your request. No additional uses are granted (such as derivative works or other editions). For any other uses, please submit a new request.

If credit is given to another source for the material you requested, permission must be obtained from that source.

[BACK](#)[CLOSE WINDOW](#)

Copyright © 2018 [Copyright Clearance Center, Inc.](#) All Rights Reserved. [Privacy statement](#). [Terms and Conditions](#).
Comments? We would like to hear from you. E-mail us at customercare@copyright.com